



CrossMark
 click for updates

Cite this: *RSC Adv.*, 2015, 5, 46981

A region-selective modified capillary microfluidic device for fabricating water–oil Janus droplets and hydrophilic–hydrophobic anisotropic microparticles†

Ke Xu,‡ Xue-Hui Ge,‡ Jin-Pei Huang, Zhu-Xi Dang, Jian-Hong Xu* and Guang-Sheng Luo

Here we developed a novel and facile microfluidic approach to produce W–O Janus droplets with a wide operating range (Ca number and volume ratio of the two dispersed phases). We then used this approach to fabricate hydrophilic–hydrophobic anisotropic Janus particles (HHAJPs). The volume ratio of the two dispersed phases and the exposure area of a specific phase could be adjusted by controlling the surfactant concentration in the continuous phase and the volume flow ratio of the two liquids. The HHAJPs could be distributed in an ordered and stable manner on oil–water interface, indicating their potential application as interface stabilizer and phase transfer catalyst.

Received 31st March 2015
 Accepted 12th May 2015

DOI: 10.1039/c5ra05690j

www.rsc.org/advances

Introduction

Anisotropic functional particles are particle materials that integrate different functions on different geometric sides, and they have been recently applied as multi-phase catalysts,^{1,2} optical pixel units,^{3–7} targeted drug release agents^{8–12} and emulsion stabilizers.^{13,14} In these fields, the synergy of their different functions enhances and broadens the applications of particles significantly.

Emulsion droplets are traditionally used as templates for micro-particle materials. For example, researchers have fabricated microbeads with different surface topographies from single-phase droplets,^{15–18} core–shell microcapsules with single and multiple cores from W/O/W or O/W/O double emulsion droplets,^{12,19–23} micro-bubbles covered by gel-films from G/W/O or G/O/W double emulsion droplets,^{24–26} and more complicated microparticles from more complicated multiple emulsion droplets.^{21,27} Janus emulsion droplets (Janus droplets) are natural templates for anisotropic particles. When the interfacial tensions in a tri-phase emulsion system with 1 continuous phase and 2 dispersed phases satisfies a certain relationship, the two dispersed-phase droplets connect to each other and form an integral ‘Janus Droplet’.^{28,29} After a solidification process, such Janus droplets become anisotropic particles. By numerical calculations, researchers have found that the

volume-ratio and exposure area ratios of the two faces could be controlled by changing the liquid volume ratio and adjusting the interfacial tension relationship, so the structure of the two faces could be controlled.^{30,31}

Traditionally, Janus droplets are produced by simply stirring three immiscible phases,^{32–34} but such a process could hardly control the uniformity of the products. Recently, microfluidic platforms have been used to realize highly controllable generation of mono-dispersed emulsion droplets,^{18,35–37} especially droplets with complicated structures.^{12,19,20,24,25,38,39} Some approaches have shown significant progress to produce uniform Janus droplets in microfluidic devices.⁴⁰ Researchers produced engulfing-structure droplets with the double-capillary method first with Janus-stable fluid system, and then the inner droplet could breakout and contact with the continuous phase, forming a Janus structure.^{40–42} However, this dynamic process for the inner droplet to contact with the continuous phase is not controllable and may be extraordinarily long if the middle phase has high viscosity (*e.g.* polymer solution or nanoparticle suspension). Therefore, some researchers developed a more controllable *in situ* method, by forming the parallel laminar flow of two dispersed phases upstream and then cutting the dual-phase laminar flow into Janus droplets with continuous phase.⁴³ This *in situ* method is considerably more controllable to produce uniform Janus droplets and then to subsequently form anisotropic particles. It has been used to synthesize anisotropic catalysts and also in medical applications.^{10,44}

However, this *in situ* method requires spontaneously stable laminar flow after two dispersed phases converged, so the operating condition has to be limited to (1) a relatively high capillary number (Ca), *e.g.* low interfacial tension between the

The State Key Lab of Chemical Engineering, Department of Chemical Engineering, Tsinghua University, Beijing 100084, China. E-mail: xujianhong@tsinghua.edu.cn; Fax: +86-10-62773017; Tel: +86-10-62773017

† Electronic supplementary information (ESI) available. See DOI: 10.1039/c5ra05690j

‡ These authors contributed equally.

dispersed phases with relatively high total flow rates, and (2) a considerably narrow volume ratio range of the two dispersed phases. Such limits in two-phase systems have been previously analysed by researchers.⁴⁵ Consequently, the current application of this method is restricted in generating O–O Janus droplets (with interfacial tension less than 1 mN m^{-1}). If the interfacial tension becomes much larger, one phase will always be cut by the other phase into droplets or plugs. This prevents its application as phase transfer catalysts and as surface-stabilizers. Even for O–O Janus droplet generation, those researchers could only produce Janus droplets with phase ratio between 1 : 5 and 5 : 1.

Here in this work, we present an essential improvement of the *in situ* method to produce water–oil Janus droplets, with a region-selective modification (RSM) of the microchannel. By modifying the wettability of selected region on the microchannel wall, the interaction between a liquid and the selected region can be adjusted. We by this way distinguished the surface into a relatively hydrophilic region and a relatively hydrophobic region. Then, the two fluids formed a parallel co-laminar flow adhering to the wall according to the responding selected modified regions till the continuous phase cut them into Janus droplets. By applying the RSM approach for the *in situ* method, we successfully expanded the *in situ* method to the systems with relatively higher interfacial tensions (from $\sim 1 \text{ mN m}^{-1}$ in previous work to $>6 \text{ mN m}^{-1}$ in this work ($\gamma_{EW} = 6.13 \text{ mN m}^{-1}$)) and larger volume-ratio ranges (from 1 : 5–5 : 1 in previous work to 1 : 10–40 : 1 in this work), and lower capillary numbers (from 10^{-2} to 10^{-1} in previous work to 10^{-4} to 10^{-1} in this work).^{46,47} Thus, we could operate the W–O system in a stable laminar flow over a considerably broadened operating range. With the tolerance of higher interfacial tensions, we could generate W–O Janus droplets *in situ* and then fabricate hydrophobic–hydrophilic anisotropic Janus particles (HHAJP). Furthermore, we found that the volume ratio of the two dispersed phase and the exposure area ratios of specific phases in the particle could be modified easily by simply adjusting the flow rate ratio of the liquids as well as by the surfactant concentration in the continuous phase.

Experimental section

Microfluidic device and materials

Here we use a two-stage capillary microfluidic device. The dispersed and continuous channels are micro-capillaries crossing in a square 20 mm long \times 20 mm wide \times 3 mm high polymethyl methacrylate (PMMA) chip. There are two capillaries used here: the first one flows the dispersed phases through the region in which the inner wall is modified and the second one flows in the continuous phase to shear the Janus droplet at the tip. They all insert into the channels in the PMMA chip, which were 1.50 mm wide \times 1.50 mm high to assure their coaxiality. The diameter of the capillaries was 1.5 mm (O.D) \times 1.05 mm (I.D). The first capillary was tapered using a micropipette puller (P-97, SUTTER Co. Ltd., USA) to form a tip with approximately a diameter of 200 μm . The two dispersed phases were injected through micro-needles with an inner diameter of 160 μm and outer diameter of 340 μm . One needle, which carries the water

phase, was placed to touch inner wall of first capillary near the tip (less than 2 mm to the tip), whereas the other one, which carries the oil phase, was in the upper middle of the capillary and far away from the tip (more than 30 mm to the tip). Thus, the water phase would stick to the wall as soon as it entered the chip, while the oil phase would have enough time to form a stable laminar flow before reaching that point. Thus, when the two phases converge, they would flow parallel through the tip to be sheared into Janus droplets. Microsyringe pumps (LSP01-1B, Baoding Longer Precise Pump Co. Ltd) were used to pump the fluidic devices. Typical orders of magnitude of the two dispersed phases and continuous phase were $10 \mu\text{L min}^{-1}$ and $1000 \mu\text{L min}^{-1}$, respectively.

We used two sets of fluids in the device: one for modification and the other for forming W–O Janus droplets. The modification system included aqueous fluids with 20 wt% NaOH and 2.0 wt% Tween 80 (surfactant), normal octane with 2 wt% Span80 (surfactant), liquid paraffin with 5 wt% Span80 (surfactant) and hexamethyldisiloxane.

The system to form W–O Janus droplets and the HHAJPs was composed of deionized water with 10 wt% poly(ethylene glycol) diacrylate monomer (PEGDA) and 0.5 wt% HMPF (photo initiator), liquid paraffin with 0.05–2.0 wt% Span80 (surfactant, the mass concentration changed when needed), and the photo-curing material ethoxylated tri-methylolpropane triacrylate monomer (ETPTA) with 0.5 wt% HMPF (photo initiator). For both of the abovementioned conditions, the needle closer to the tip carried the water phase, whereas the other needle far away from the tip carried the oil phase. Table 1 shows the interfacial tensions of the different systems.

Torza and Mason^{46,47} used the spreading coefficient (S_i) to predict the morphology of three fluids as follows:

$$S_i = \sigma_{jk} - (\sigma_{ij} + \sigma_{ik}) \quad (i \neq j \neq k = 1, 2, 3),$$

σ_{jk} represent the interfacial tension between j and k fluids.

$$S_1 < 0 \quad S_2 < 0 \quad S_3 > 0, \text{ engulfing structure}$$

$$S_1 < 0 \quad S_2 < 0 \quad S_3 < 0, \text{ Janus structure}$$

$$S_1 < 0 \quad S_2 > 0 \quad S_3 < 0, \text{ separating structure}$$

here in our work, the interfacial tensions of the three fluids were diverse because we used a continuous phase with different mass fractions of surfactant. We used all data to calculate the

Table 1 The interfacial tensions of the different systems

Mass fraction of Span80 (wt%)	γ_{EW} (mN m^{-1})	γ_w (mN m^{-1})	γ_E (mN m^{-1})
0.05	6.13	4.89	3.47
0.1	6.13	4.34	3.49
0.15	6.13	4.27	3.5
0.5	6.13	4.12	3.53
1	6.13	3.77	3.48
2	6.13	2.71	3.47

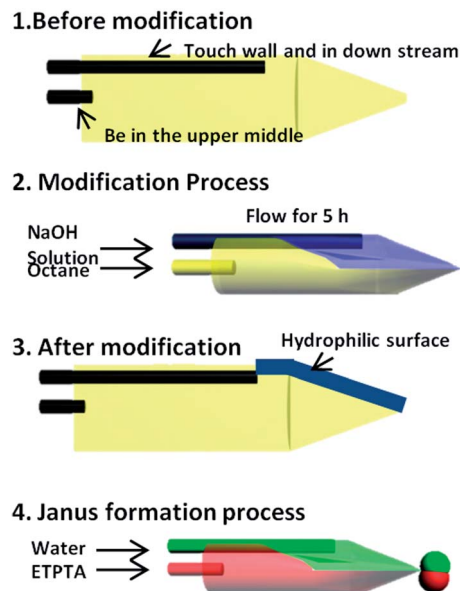
spreading coefficient, as shown in Table 2. It shows that we can produce W–O Janus droplet with different structures by using these systems.

The generated Janus droplets were polymerized and solidified into ETPTA and hydrogels composed of PEGDA under a UV point light source (LC8, Model L9588-01, Hamamatsu) exposure for 10 seconds. ETPTA is hydrophobic, whereas the hydrogel is hydrophilic, and thus we obtained the HHAJPs. The chemicals used were chemically pure and purchased from Bai Ling Wei and Sigma corporations.

We used an optical microscope (BX61, Olympus) assembled with a high speed camera (DK-2740, Dantech) to take micro-photographs and movies. We also used a dynamic interfacial tension measurement instrument (OCAH200, DataPhysics Instruments GmbH, Germany) to utilize the pendant drop method and the contacting angle method to measure the interfacial tensions of the experimental systems and the contact angles of capillary inner walls before and after hydrophilic modification. We also used SEM to observe the surface of the wall to find the mechanism of modification.

Region-selective modification process

Here we propose a novel RSM process and the construction of a parallel hydrophobic–hydrophilic pathway for the two inner phases. Scheme 1 shows the process step by step. First, we place two needles at the separate positions, as shown in Scheme 1.1, and then immerse the micro-device into hexamethyldisiloxane for 5 hours at 80 °C to make the capillary overall hydrophobic and ETPTA-wetting. Second, an aqueous solution containing NaOH and surfactant is injected through the needle touching the inner wall after the oil phase flowing through the other needle and occupied the channel. With high flow rates of both liquids, which leads to a high Ca condition, we formed a steady co-laminar flow in the dispersed-phase tube. After continuously flowing for 5 hours, NaOH reacts with the capillary wall and makes the contacting region water-wetting while keeping the rest of the surface ETPTA-wetting. Third, we stopped flowing the modifying fluids and obtained a selective region to be hydrophilic (the blue region in Scheme 1.3) while other parts remain hydrophobic. We then inject Janus formation fluids, *i.e.* water and ETPTA. Because of the difference in wettability of the inner wall towards water and ETPTA, we obtain two parallel pathways for the aqueous phase and the ETPTA phase, and they were then sheared simultaneously at the tip by the continuous phase fluid.



Scheme 1 A brief scheme of the RSM process step by step. (1) Capillary assembly. We put two needles into the micro-capillary as the dispersed phase channels and modified the overall capillary into hydrophobic and ETPTA-wetting. (2) Modifying fluids injection. An aqueous solution containing NaOH and surfactant is injected through a needle touching the inner wall after oil (octane) occupying the channel with high flow rates of both liquids to form a steady co-laminar flow in the dispersed-phase tube. This modification process lasted for 5 hours. (3) After RSM. We obtained a selective region (the blue region) to be hydrophilic while other parts remain hydrophobic. (4) Generating Janus droplets. Working system which are water phase and ETPTA are injected into the device after RSM process to form stable parallel laminar flow and to be sheared at the tip by continuous phase to form Janus droplet.

Through this procedure, we obtained W–O Janus droplets by an *in situ* method after RSM.

Results and discussions

Modification result of the capillary inner wall

After modification, the wettability of the inner channel wall was adjusted. A water-wetting pathway was formed on the ETPTA-wetting capillary wall from the aqueous phase needle tip to the capillary orifice. Then, we compared the contact angle between the water and inner wall before and after NaOH solution modification. First, we modified two glass slides to be hydrophobic using the same method as shown in Scheme 1.1, and then further modified one using an NaOH solution to become hydrophilic. Then we measured the contact angles of the water droplet on the two glass slides in an ETPTA solution. The comparison result is shown in Fig. 1b, where we find the contact angle is 169.9° on ETPTA-wetting glass (glass only modified by hexamethyldisiloxane) and 52.1° on hydrophilic glass (glass first modified by hexamethyldisiloxane and then by the NaOH aqueous solution), which suggest increase in the hydrophilic wettability. The SEM pictures shown in Fig. 1c and d indicate that the glass surface is considerably modified, full of

Table 2 The spreading coefficients of different systems

Mass fraction of Span80 (wt%)	S_1	S_2	S_3
0.05	−7.55	−2.23	−4.71
0.1	−6.98	−1.7	−5.28
0.15	−6.9	−1.64	−5.36
0.5	−6.72	−1.52	−5.54
1	−6.42	−1.12	−5.84
2	−5.37	−0.05	−6.89

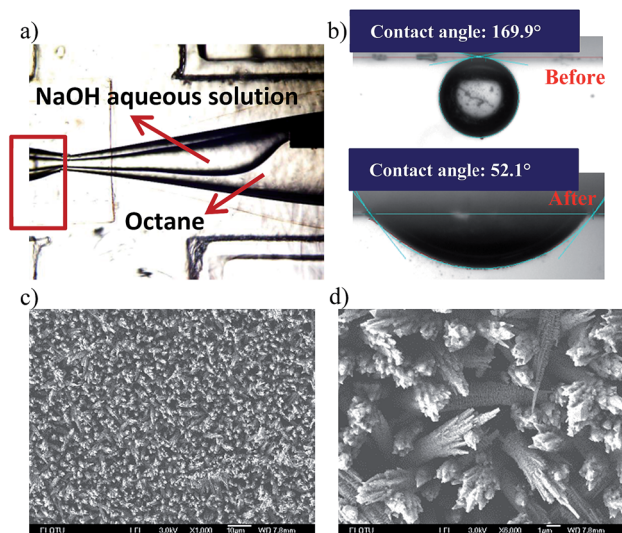


Fig. 1 The microscopic image of hydrophilic modification process and the modification effect comparison. (a) The microscopic image of the hydrophilic modification process. The NaOH and octane formed co-laminar flow in the dispersed tube. The red square is the collecting tube to invert the NaOH aqueous solution to interact with the continuous tube. It just exists temporarily in this step. (b) The comparison of contact angles between capillary and water in ETPTA monomer before (169.9°) and after hydrophilic modification (52.1°). (c) The SEM pictures of the glass surface after modification. (d) The magnification of specific part of the surface. The surface is eroded severely by the NaOH aqueous solution. The black bar represents $200\ \mu\text{m}$.

ravines due to NaOH solution corrosion. In experiments, we found that the modification would maintain effective for more than 10 days.

Formation of droplets

The schematic diagram of synthesis process of Janus emulsion droplets and particles is shown in Scheme 1.4. In the microfluidic device downstream from the RSM process region, we formed stable and controllable Janus emulsions. A movie of Janus droplet formation is in the ESI (Movie S1-formation process[†]).

The growing, cutting and flowing process is shown in Fig. 2a. If we solidify the generated Janus droplets *in situ* under UV exposure, we could get HHAJPs. Fig. 2b and c show the Janus droplet in the channel and Janus particles after solidification in which we show that the HHAJPs were highly monodispersed.

During the formation process, we studied the flow rates range to form stable Janus droplets. ETPTA and water fluids formed a parallel co-laminar flow and were sheared by the continuous phase to form one water semi-sphere droplet sticking to one ETPTA semi-sphere droplet. We call this Janus droplet a “single Janus droplet”, as shown in Fig. 3a. Apart from this, we observed another stable flowing pattern. When the two phases stayed longer in the tip while the flow rate of water phase was high, there would be multiple water droplets formed and stuck to one ETPTA droplet, forming a multiple Janus structure, and we called that “Multiple Janus” as shown in Fig. 3b. Here in this work, we focus on the single Janus droplet.

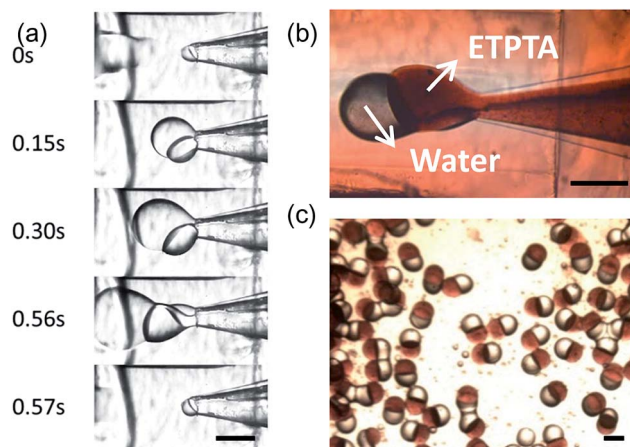


Fig. 2 The microscopic images of the synthesis of mono-dispersed Janus droplets: (a) Janus droplet formation process. Oil and water phase formed co-laminar flow and adhered together to flow out from the tip, then the integral drop grew bigger until it was sheared at the tip to form a Janus droplet. (b) The colourful Janus droplet. The red part represents oil phase (ETPTA) and the colourless phase represents water phase. (c) Janus particles after solidification. They are mono-dispersed. The scale bars above represent $500\ \mu\text{m}$.

We further explored the relationship between the two Janus structures and the flow rates to find out the flow rates scope to form stable single Janus. Fixing the continuous flow rates as $1\ \text{mL}\ \text{min}^{-1}$ and $1.6\ \text{mL}\ \text{min}^{-1}$, we changed the flow rates of the ETPTA and water phases. The results showed that a relatively high continuous flow rate could help to avoid multiple Janus droplets, as shown in Fig. 3c and d.

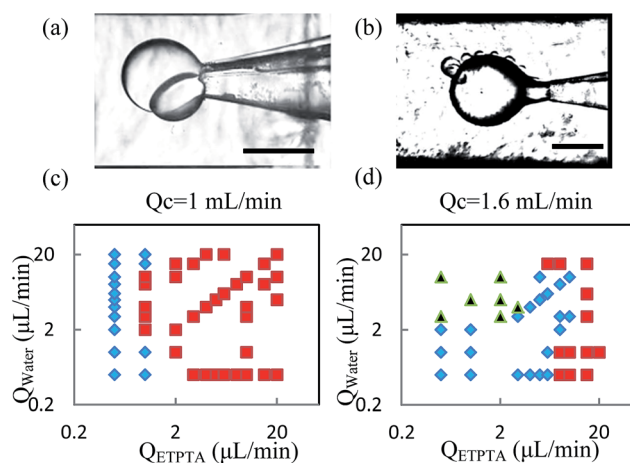


Fig. 3 The two flow patterns of Janus droplets: single Janus and multiple Janus and their formation condition. (a) Single Janus. One water and one ETPTA droplet form together. (b) Multiple Janus. Many small water droplets adhere to one ETPTA droplet. (c) and (d) The relationship between Janus structure and the flow rates for different flow rates of the continuous phase. Red squares represent multiple Janus is formed in the corresponding flow rates, blue rhombus represent rates at which single Janus is formed at the corresponding flow, and the black triangle represent an unstable state in which the formation changed between single Janus and multiple Janus. The black bars represent $500\ \mu\text{m}$.

Enlargement of the operation range

The operation range of our RSM method is considerably enlarged compared with previous *in situ* methods without RSM, because the RSM reduces the difficulty to get stable laminar flow in a dispersed-phase channel. Both the restrictions in interfacial tension and in volume ratio are reduced considerably. The flow rate in the dispersed-phase channel could be operated at a 2-order lower Ca condition than in previous work. The volume ratio of the two dispersed phases is also extended considerably. Table 3 and Fig. 4 show the comparison between our work and previous work. To elaborate on the advantages of our work more clearly, we show the picture from a ref. 43 in Fig. 4b and analyse our data in the same way. The blue circle region represents the parameters in which we could obtain stable Janus droplets and the corresponding Ca number. From the comparison, we find that we could produce stable droplets at a lowest Ca number equal to 0.0001, while in the reference, they could only form stable droplets when the Ca number was more than 0.01, and this shows our significant improvement in the Ca number. Thus, we could synthesis in lower flow rates and higher interfacial tension. This improvement allows us to produce HHAJPs composed of water and oil phases (which would have higher interfacial tension) at a larger flow rate range (from low flow rates to high rates).

Precise control of the Janus droplets' size and structure

Moreover, we could control the size and structure of the Janus droplets precisely by adjusting the flow rates and changing the interfacial tension. Fig. 5 show the structure change of the Janus emulsion when the flow-rate ratio of the two phases changes. They are all Janus particles, but they have different volume ratios of hydrophilic semi-sphere to hydrophobic semi-sphere. Fig. 5a–c are the micrographs showing particles formed when the flow-rate ratio of water to ETPTA was changed from 1 : 10 to 10 : 1. We can see that when the flow rates of the two phases were the same, the semi-sphere of each phase almost have the same volume. Actually, the ratio is not 1 : 1 and it is related to the interfacial tensions of the three phases³¹ because of the deformation between the two dispersed phases when they touch. Here, when we ignored the influence of the deformation and assumed the dispersed phase as a spherical crown, we find that the diameter ratio of the two spherical crowns increased with the increase of the flow rate ratio, as shown in Fig. 5d. Through this relationship, we adjusted the size of each part of the HHAJPs by adjusting the flow rates of each phase.

Table 3 The comparison of the operating ranges of this work and previous work

	Unmodified ^{43,44}	Modified
Interfacial tension	<1 mN m ⁻¹	6 mN m ⁻¹
Inner phase ratio	0.2–5	0.1–40
Ca number	10 ⁻² to 10 ⁻¹	10 ⁻⁴ to 10 ⁻¹

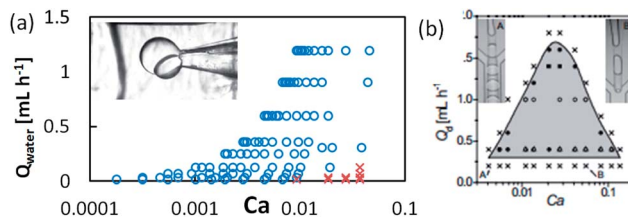


Fig. 4 The comparison of Ca number range between our work and previous work to show the enlargement of operation range in our work. (a) The relationship with the flow rates to the Ca number in our work. The blue circle represents stable single droplets, and the red cross represents unstable droplets. It shows the stable range of the Ca number varies from 0.0001 to 0.01. (b) The citation of previous work as comparison.⁴³ The stable range of Ca number here was from 0.01 to 0.1.

Morphology control based on the change of interfacial tensions

For some applications, like in the catalysis field, the exposure area is more important than the volume and considerable research is devoted for achieving the highest exposure area of a certain phase, *i.e.*, the highest specific area. In our work, we succeeded in finding an easy way to adjust the specific area. When keeping the volumes of the two phases constant, we found the exposure areas of each phase could be highly controlled by simply changing the interfacial tension. In our work, we adjusted the surfactant concentration in the continuous phase to adjust the interfacial tension between water phase and the continuous phase. Fig. 6a–c show the different exposure areas of the hydrophilic phase (black part of HHAJPs) when the surfactant (Span80) concentration is varied. This change was seen because the surfactant changed the interfacial tension, which in turn changed the contact angles between the three phases. Therefore, for the same volume ratio, the

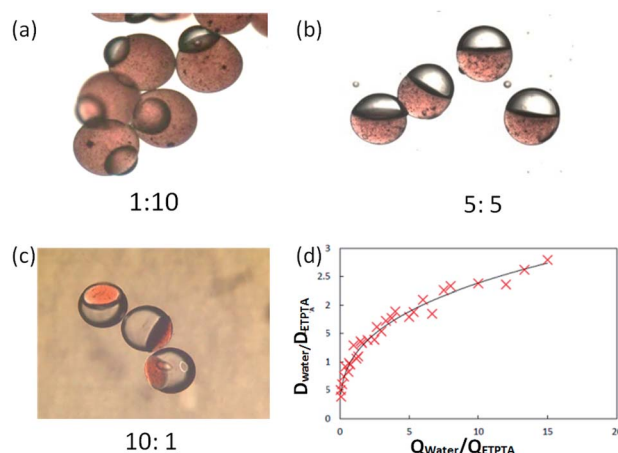


Fig. 5 The relationship of the dimension ratio of Janus semi-spheres with the flow-rate ratio of the corresponding fluids. (a) to (c) The micrographs of Janus particles with different flow-rate ratios of water to ETPTA phase: (a) 1 : 10, (b) 1 : 1 and (c) 10 : 1. The scale bar represents 500 μ m. (d) The relationship of the $D_{\text{water}}/D_{\text{ETPTA}}$ and $Q_{\text{water}}/Q_{\text{ETPTA}}$; they are positively correlated but they are not linearly dependent. The red cross represents the experiment data.

encapsulation part of the hydrophilic phase was different. Fig. 6a shows the extreme case in which the hydrophilic phase was almost engulfed by the other phases. As shown in Fig. 6b, the major part of the hydrophilic phase was encapsulated, while as shown in Fig. 6c, only a minor amount of the hydrophilic phase was encapsulated, which means the exposure area rises when the surfactant concentration increases. Fig. 6d and e demonstrates how the interfacial tension changed when the surfactant concentration changed. For water and liquid paraffin (continuous phase), the interfacial tension between them decreased as the Span80 concentration in the liquid paraffin increased. After the concentration increased to the critical micelle concentration (CMC), the increase of the concentration did not decrease the interfacial tension. As for the ETPTA and liquid paraffin (continuous phase), because they are both oil, the surfactant had only a scarce effect on their interfacial tension, so the interfacial tension almost stayed unchanged during the whole process. Fig. 6e shows that the contact angles changed with the Span80 mass concentration. When neglecting gravity (because our droplets are small), the interfacial tension would balance to zero according to the Neumann's triangle at the three-phase boundary. The contact angles between each two-phase system were determined by their interfacial tensions. Here, α represents the contact angle between water and liquid paraffin, β represents the contact angle between ETPTA and liquid paraffin, and δ represents the contact angle between water and ETPTA. γ_W represents the interfacial tension between water and liquid paraffin, γ_E represents the interfacial tension between ETPTA and liquid paraffin, and γ_{EW} represents the interfacial tension between water and ETPTA. Their schematic plot is shown in Fig. 6e and their relationship meets the following equations:

$$\alpha = a \cos[0.5(\gamma_W^2 + \gamma_{EW}^2 - \gamma_E^2)/(\gamma_W \times \gamma_{EW})] \quad (1.1)$$

$$\beta = a \cos[0.5(\gamma_W^2 + \gamma_E^2 - \gamma_{EW}^2)/(\gamma_W \times \gamma_E)] \quad (1.2)$$

$$\delta = a \cos[0.5(\gamma_E^2 + \gamma_{EW}^2 - \gamma_W^2)/(\gamma_E \times \gamma_{EW})] \quad (1.3)$$

From Fig. 6e, we find that when the Span80 mass concentration increased (the interfacial tension decreased according to Fig. 6d), all contact angles changed, where α decreased and β and δ increased, and thus the exposure area of the hydrophilic phase increased. Because the volume of the water phase was fixed, after normalizing the volumes of all phases (thus the mass concentration of Span80 is transformed to the mass fraction), the exposure area was equal to the specific area. Then, we determined the relationship of the specific surface area of the hydrophilic phase and the mass fraction of Span80. From Fig. 6f, we could find that the specific surface area increases fast when mass fraction of Span80 increased until reaching the CMC. Such a method allows us to minimize the amount of some expensive materials when keeping a relatively high surface area, which is of significance in some areas such as catalysis and interfacial stabilization where the exposure area determines the efficiency and the volume

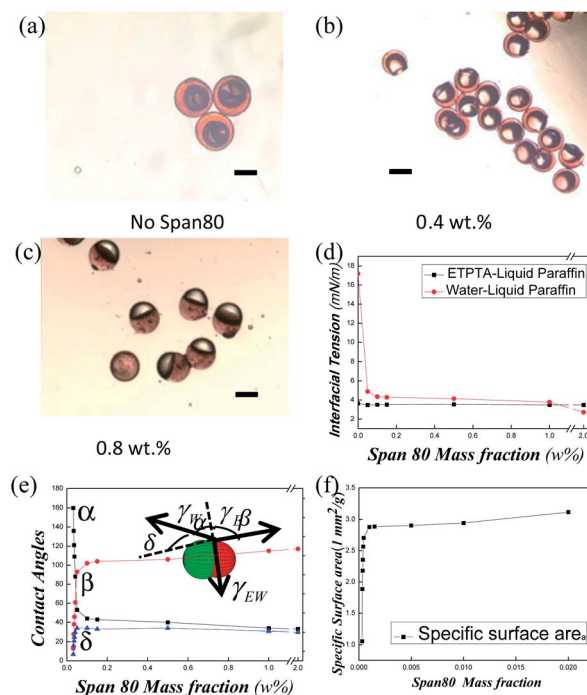


Fig. 6 The exposure surface area adjustment of hydrophilic phase. (a–c) The micrographic images of Janus droplets with the concentration of Span80 in the outer phase changing from (a) 0%, (b) 0.4 wt%, (c) 0.8 wt%, respectively. (d–f) The interfacial tensions, the contact angles and the specific exposure areas of the ETPTA phase changed with the concentration of Span80. The scale bar represents 200 μm . Hydrophilic–hydrophobic anisotropic microparticles dispersion in oil–water interface.

determines the cost. High specific exposure surface areas of an expensive material are always more economical.

Furthermore, we tested the hydrophilic–hydrophobic property of the HHAJPs. When we put about 200 HHAJPs into a mixture of 20 g octanol and 3 g water and shook it for about 30 seconds, we found that all of the HHAJPs are adsorbed and directionally distributed on the oil–water interface, with the ETPTA side immersed in the octanol and the PEGDA side

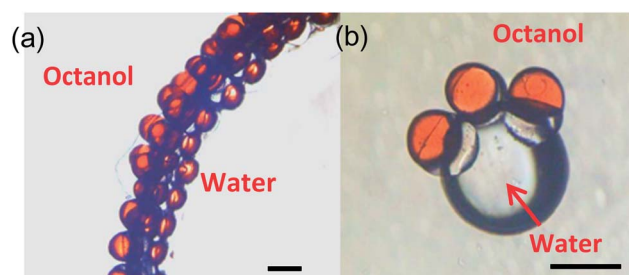


Fig. 7 The HHAJPs oriented and adsorbed on the water–oil interface. (a) Many particles dispersed at the interface of octanol and water. (b) Several HHAJPs scattered on the surface of a water drop. The red part of the HHAJPs represents the oil phase (ETPTA) and the colourless part represents the water phase (PEGDA hydrogel). When dispersed on the surface, the oil phase always orients towards octanol, whereas the water phase orients towards the water. The scale bar represents 200 μm .

immersed in the water side. These particles packed closely and covered the interface, similar to the behaviour of a solid surfactant. Fig. 7 shows the microscopy images of the dispersion. Fig. 7a shows that the particles were orderly scattered at the interface. The red part represents the hydrophobic phase, and they are all directed to the octanol, whereas the other part, which could not be seen clearly because it was covered by the boundary of the octanol and water, represents the hydrophilic phase and they all are directed to the water. From Fig. 7b, we can see the dispersion of phases more clearly. It depicts three HHAJPs scattered along a water droplet surface with the octanol environment. The red part of the HHAJP (hydrophobic phase) directs towards octanol, whereas the colourless part (hydrophilic phase) directs towards water. Such a property of HHAJPs makes them promising in phase transfer catalysis applications.

Conclusions

In summary, by regional selective modification (RSM) technology, we improved the *in situ* generation of W–O Janus droplets in a microfluidic device and successfully obtained monodispersed water–oil Janus droplets and hydrophobic–hydrophilic anisotropic Janus particles (HHAJPs). Compared with previous work, the improved method allows a considerably higher interfacial tension between two dispersed phases, a larger volume ratio range, and a larger Ca range. The size of HHAJPs could be precisely controlled. By adjusting the surfactant concentration in the continuous phase, the exposure surface area could be optimized, which allows us to use the least amount of some expensive dispersed phase to gain a specific exposure area. Such HHAJPs can directionally distribute on the oil–water interface stably, indicating a potential application as an interface stabilizer and phase transfer catalyst.

Acknowledgements

The authors gratefully acknowledge the supports of the National Natural Science Foundation of China (21322604, 21476121) and Tsinghua University Initiative Scientific Research Program (2014z21026).

Notes and references

- 1 T. Brugarolas, B. J. Park, M. H. Lee and D. Lee, *Adv. Funct. Mater.*, 2011, **21**, 3924–3931.
- 2 J. Faria, M. P. Ruiz and D. E. Resasco, *Adv. Synth. Catal.*, 2010, 2359–2364.
- 3 Y. Hu, J. Wang, C. Li, Q. Wang, H. Wang, J. Zhu and Y. Yang, *Langmuir*, 2013, **29**, 15529–15534.
- 4 S.-H. Kim, S.-J. Jeon, W. C. Jeong, H. S. Park and S.-M. Yang, *Adv. Mater.*, 2008, **20**, 4129–4134.
- 5 M. Marquis, D. Renard and B. Cathala, *Biomacromolecules*, 2012, **13**, 1197–1203.
- 6 S. Seiffert, M. B. Romanowsky and D. A. Weitz, *Langmuir*, 2010, **26**, 14842–14847.
- 7 S. N. Yin, C. F. Wang, Z. Y. Yu, J. Wang, S. S. Liu and S. Chen, *Adv. Mater.*, 2011, **23**, 2915–2919.
- 8 Y. Chen, G. Nurumbetov, R. Chen, N. Ballard and S. A. Bon, *Langmuir*, 2013, **29**, 12657–12662.
- 9 Y. Ning, C. Wang, T. Ngai, Y. Yang and Z. Tong, *RSC Adv.*, 2012, **2**, 5510.
- 10 N. Prasad, J. Perumal, C.-H. Choi, C.-S. Lee and D.-P. Kim, *Adv. Funct. Mater.*, 2009, **19**, 1656–1662.
- 11 R. K. Shah, J.-W. Kim and D. A. Weitz, *Adv. Mater.*, 2009, **21**, 1949–1953.
- 12 X.-H. Ge, J.-P. Huang, J.-H. Xu and G.-S. Luo, *Lab Chip*, 2014, **14**, 4451–4454.
- 13 B. Liu, J. Liu, F. Liang, Q. Wang, C. Zhang, X. Qu, J. Li, D. Qiu and Z. Yang, *Macromolecules*, 2012, **45**, 5176–5184.
- 14 Z. Nie, S. Xu, M. Seo, P. C. Lewis and E. Kumacheva, *Langmuir*, 2010, **26**, 11732–11736.
- 15 S. Liu, R. Deng, W. Li and J. Zhu, *Adv. Funct. Mater.*, 2012, **22**, 1692–1697.
- 16 G. T. Vladisavljević, I. Kobayashi and M. Nakajima, *Microfluid. Nanofluid.*, 2012, **13**, 151–178.
- 17 J. H. Xu, H. Zhao, W. J. Lan and G. S. Luo, *Adv. Healthcare Mater.*, 2012, **1**, 106–111.
- 18 K. Xu, J.-H. Xu, Y.-C. Lu and G.-S. Luo, *Cryst. Growth Des.*, 2013, **13**, 926–935.
- 19 N. N. Deng, W. Wang, X. J. Ju, R. Xie, D. A. Weitz and L. Y. Chu, *Lab Chip*, 2013, **13**, 4047–4052.
- 20 M. H. Lee, K. C. Hribar, T. Brugarolas, N. P. Kamat, J. A. Burdick and D. Lee, *Adv. Funct. Mater.*, 2012, **22**, 131–138.
- 21 L. Liu, W. Wang, X.-J. Ju, R. Xie and L.-Y. Chu, *Soft Matter*, 2010, **6**, 3759.
- 22 G. T. Vladisavljević, H. C. Shum and D. A. Weitz, *Colloid Polym. Sci.*, 2012, 115–118.
- 23 W. Wang, M. J. Zhang, R. Xie, X. J. Ju, C. Yang, C. L. Mou, D. A. Weitz and L. Y. Chu, *Angew. Chem.*, 2013, **52**, 8084–8087.
- 24 H. Chen, J. Li, J. Wan, D. A. Weitz and H. A. Stone, *Soft Matter*, 2013, **9**, 38.
- 25 R. Chen, P. F. Dong, J. H. Xu, Y. D. Wang and G. S. Luo, *Lab Chip*, 2012, **12**, 3858–3860.
- 26 W.-T. Wang, R. Chen, J.-H. Xu, Y.-D. Wang and G.-S. Luo, *RSC Adv.*, 2014, **4**, 16444.
- 27 J.-H. Xu, X.-H. Ge, R. Chen and G.-S. Luo, *RSC Adv.*, 2014, **4**, 1900.
- 28 J. Guzowski, P. M. Korczyk, S. Jakiela and P. Garstecki, *Soft Matter*, 2012, **8**, 7269.
- 29 S. E. Friberg, I. Kovach and J. Koetz, *ChemPhysChem*, 2013, **14**, 3772–3776.
- 30 L. Ge, S. Lu and R. Guo, *J. Colloid Interface Sci.*, 2014, **423**, 108–112.
- 31 H. Hasinovic, S. E. Friberg and G. Rong, *J. Colloid Interface Sci.*, 2011, **354**, 424–426.
- 32 I. Kovach, J. Koetz and S. E. Friberg, *Colloids Surf., A*, 2014, **441**, 66–71.
- 33 J. Tan, J. H. Xu, S. W. Li and G. S. Luo, *Chem. Eng. J.*, 2008, **136**, 306–311.
- 34 K. Xu, C. P. Tostado, J. H. Xu, Y. C. Lu and G. S. Luo, *Lab Chip*, 2014, **14**, 1357–1366.

- 35 J. Xu, S. Li, C. P. Tostada, W. Lan and G. Luo, *Biomed. Microdevices*, 2008, **2009**, 243–249.
- 36 A. Abate, A. Poitzsch, Y. Hwang, J. Lee, J. Czerwinska and D. Weitz, *Phys. Rev. E: Stat., Nonlinear, Soft Matter Phys.*, 2009, 80.
- 37 Y. Zhao, Z. Xie, H. Gu, L. Jin, X. Zhao, B. Wang and Z. Gu, *NPG Asia Mater.*, 2012, **4**, e25.
- 38 K. Xu, J.-h. Xu, Y.-c. Lu and G.-S. Luo, *Cryst. Growth Des.*, 2014, **14**, 401–405.
- 39 T. Tanaka, M. Okayama, H. Minami and M. Okubo, *J. Am. Chem. Soc.*, 2005, 8058–8063.
- 40 C. H. Chen, R. K. Shah, A. R. Abate and D. A. Weitz, *Langmuir*, 2009, **25**, 4320–4323.
- 41 T. Nisisako and T. Torii, *Adv. Mater.*, 2007, **19**, 1489–1493.
- 42 W. Lan, S. Li, J. Xu and G. Luo, *Microfluid. Nanofluid.*, 2012, **13**, 491–498.
- 43 J. H. Xu, G. S. Luo, S. W. Li and G. G. Chen, *Lab Chip*, 2006, **6**, 131–136.
- 44 B. Zhao, J. S. Moore and D. J. Beebe, *Science*, 2001, **291**, 1023–1026.
- 45 A. Hibara, S. Iwayama, S. Matsuoka, M. Ueno, Y. Kikutani, M. Tokeshi and T. Kitamori, *Anal. Chem.*, 2005, 943–947.
- 46 S. Torza and S. Mason, *Science*, 1969, **163**, 813.
- 47 S. Torza and S. Mason, *J. Colloid Interface Sci.*, 1970, **33**, 67–83.